# Giant dipole resonance in very hot nuclei of mass $A \approx 115$

T. Suomijärvi,[1] Y. Blumenfeld,[1] P. Piattelli,[2] J. H. Le Faou,[1] C. Agodi,[2] N. Alamanos,[3] R. Alba,[2] F. Auger,[3] G. Bellia,[2,*] Ph. Chomaz,[4] R. Coniglione,[2] A. Del Zoppo,[2] P. Finocchiaro,[2] N. Frascaria,[1] J. J. Gaardhøje,[5] J. P. Garron,[1] A. Gillibert,[3] M. Lamehi-Rachti,[1,†] R. Liguori-Neto,[3,‡] C. Maiolino,[2] E. Migneco,[2,*] G. Russo,[2,*] J. C. Roynette,[1] D. Santonocito,[2] P. Sapienza,[2] J. A. Scarpaci,[1] and A. Smerzi[2]

[1]*Institut de Physique Nucléaire, IN$_2$P$_3$-CNRS, 91406 Orsay, France*

[2]*INFN-Laboratorio Nazionale del Sud, Via S. Sofia 44, 95123, Catania, Italy*

[3]*SPhN, DAPNIA, CEN Saclay, 91191 Gif sur Yvette, France*

[4]*GANIL, BP 5027, 14021 Caen, France*

[5]*The Niels Bohr Institute, University of Copenhagen, DK-2100 Ø, Denmark*

(Received 8 December 1995)

Gamma rays, light charged particles, and evaporation residues emitted from hot nuclei formed in the $^{36}$Ar+$^{90}$Zr reaction at 27 MeV/nucleon have been measured at the GANIL facility with the $4\pi$ barium fluoride multidetector MEDEA. The combination of the residue and particle measurements shows that nuclei with masses around 115 and excitation energies between 350 and 550 MeV are produced. The $\gamma$ spectra measured in coincidence with the evaporation residues exhibit three components: a low-energy statistical component, a high-energy contribution due to nucleon-nucleon bremsstrahlung during the initial stages of the collision, and a contribution from the decay of the giant dipole resonance built on highly excited states. The characteristics of the bremsstrahlung component are in agreement with previously published systematics. The $\gamma$ yield from the decay of the giant dipole resonance remains constant over the excitation energy range studied. A comparison with other experiments shows that the $N/Z$ asymmetry in the entrance channel does not affect the $\gamma$ yield. Statistical calculations performed using the code CASCADE and supposing a fixed width and full sum rule strength for the dipole resonance strongly overpredict the data. The hypothesis of a continuously increasing width of the resonance with temperature gives a better agreement with experiment near the centroid of the resonance but overpredicts the $\gamma$ spectra at higher energies. The best account of the data is given by assuming a cutoff of $\gamma$ emission from the resonance above an excitation energy of approximately 250 MeV. This cutoff is discussed in terms of the time necessary to equilibrate the dipole oscillations with the hot compound nucleus. Finally, some evidence is given for a possible new low-energy component of the dipole strength at very high temperatures. [S0556-2813(96)05505-7]

PACS number(s): 24.30.Cz, 25.70.Gh, 25.70.Ef

## I. INTRODUCTION

A spectacular and well-established result of nuclear physics is the presence of giant resonance (GR) modes in nuclei [1], which demonstrates the persistence of strongly collective excitations in fermionic systems with a small number of constituents. A natural question that arises is the evolution of such collective motion of nucleons in highly excited nuclei, which are presumptively chaotic systems. The field of the study of giant resonances built on excited nuclear states was launched in 1955 by Brink [2], who proposed that giant resonances could be built on all nuclear states, and that their properties should not depend significantly on the nuclear state. Experimental investigations have focused on the giant dipole resonance (GDR), which has a sizable $\gamma$-decay branch, of the order of $10^{-3}$, allowing a rather straightforward measurement of its characteristics. The first experimental observation of a GR built on an excited state was reported in a proton capture $(p,\gamma)$ experiment on $^{11}$B where the GDR built on the first excited state of $^{12}$C was observed [3]. From subsequent $(p,\gamma)$ experiments on various other light nuclei [4] emerged a coherent picture supporting the Brink hypothesis. The field fully matured with the use of heavy ion beams, which offer the possibility, through fusion reactions, to study the GDR built on highly excited continuum states in a large variety of nuclei [5]. Above the bombarding energies where complete fusion is the dominant reaction mechanism, it is possible to produce even hotter compound nuclei through either incomplete fusion or deep inelastic reactions. The measurement of $\gamma$ rays emitted from nuclei formed by both these reaction mechanisms has yielded information on the characteristics of the GDR built on continuum states with excitation energies reaching as high as 5 MeV/nucleon [6]. At moderate excitation energies ($E^* < 2$ MeV/nucleon), the characteristics of the GDR will provide insight into the shapes and fluctuations of hot nuclei. At higher temperatures, one may expect to probe the limits of collective motion in nuclei, and obtain information on the time scales for equilibration and decay of highly excited nuclear species.

The most extensive systematics concerning the GDR built on continuum states have been established for nuclei of mass around 110, which have near spherical ground states. When account is taken for eventual ground state deformation, results for other mass regions can be considered as similar. In the remainder of the paper we will concentrate on the mass 110 region.

[*]Also at Dipartimento di Fisica dell'Università, Catania, Italy.

[†]On leave from University of Teheran, Iran.

[‡]On leave from University of São Paolo, Brazil.

 

The GDR can be characterized through three parameters, its centroid energy $E$, width $\Gamma$, and sum-rule strength $S$, expressed as a percentage of the Thomas-Reiche-Kuhn sum rule (TRKSR). The characteristics of the GDR built on the ground state have been well known for several decades through $(\gamma,n)$ reactions [7]. For spherical nuclei, the line shape of the GDR can be represented by a single Lorentzian function. In the case of $^{110}$Sn the parameters are centroid energy $E_0 = 16$ MeV, width $\Gamma_0 = 4.8$ MeV, and strength $S = 100\%$ of the TRKSR. To briefly review the case of the GDR built on hot nuclei, we will divide, for experimental reasons, the excitation energy scale into three regions: below 130 MeV, between 130 and 300 MeV, and above 300 MeV.

For moderately hot nuclei in the first region, the experimental characteristics of the GDR are now well established [6]: The centroid energy remains practically constant at 15 MeV, the width increases up to about 12 MeV at 130 MeV excitation energy, and full sum-rule strength is retained. Since the nuclei studied are formed in complete fusion reactions, it seems logical to associate the increasing GDR width with the increase of the maximum angular momentum populated in the reaction, which will influence the deformation of the excited nuclei [8]. Recent experimental studies, where a spin spectrometer was used in order to select different initial angular momenta, seem to corroborate this interpretation [9]. Thermal effects may also contribute to the width increase, as shown in studies using inelastic scattering of $\alpha$ particles to excite the GDR in nuclei with very low angular momentum [10]. In the recent work of Pierroutsakou *et al.* [11], using heavy ion fusion reactions, the data are fitted just as well supposing an evolution of the GDR width dominated by angular momentum or excitation energy effects.

For hotter nuclei between 130 and 300 MeV, the centroid energy and percentage of the TRKSR still remain constant, whereas different analyses have yielded divergent results concerning the evolution of the GDR width. Experiments by Bracco *et al.* [8] and more recently Hoffmann *et al.* [12], using fusion reactions, and Enders *et al.* [13], where the excited nuclei are produced in deep-inelastic collisions, led to the conclusion of a saturation of the width at a value around 12 MeV. This behavior would be in line with the assumption that the evolution of the width is dominated by angular momentum effects, since the maximum angular momentum that a Sn nucleus can sustain before fission is reached in reactions producing Sn nuclei at 130 MeV excitation energy [8]. Yoshida and co-workers [14,15] have fitted their results with a continuously increasing width. Such an evolution is supported by theoretical calculations based on the Landau-Vlasov equation [16,17], where the increase of nucleon-nucleon collisions with temperature results in a broadening of the resonance.

While the $\gamma$-ray multiplicity from GDR decay increases up to 300 MeV excitation energy, in agreement with 100% sum-rule strength, this seems no longer to be the case at higher energies, where a saturation of the $\gamma$ yield has been observed [14,15,18,19]. One possible explanation for this saturation would be a rapid continuous increase of the GDR width with temperature [16,17,20]. GDR $\gamma$ rays would then be spread over a very large energy range and thus contribute very little to the region near the centroid of the resonance [14,15]. Alternatively, this saturation may be an indication of a loss of collectivity of very hot nuclei [18,21]. A hindrance of the $\gamma$ emission due to the time necessary to couple the GDR to the compound nucleus has also been invoked [22].

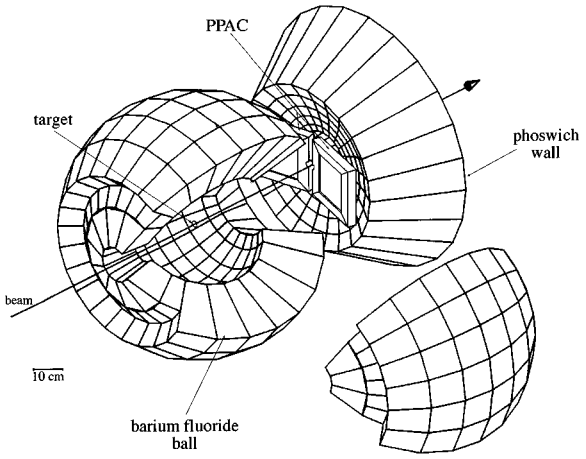


FIG. 1. View of the experimental setup showing the MEDEA detector and the two forward PPAC's.

In order to investigate in detail the open questions concerning the width and strength of the GDR in nuclei around mass 110, at excitation energies above 300 MeV, we have measured the $\gamma$-ray emission from $^{36}$Ar+$^{90}$Zr collisions at 27 MeV/nucleon. At such a high bombarding energy, complete fusion, if it persists at all, makes up only a very small part of the reaction cross section. Therefore the experimental setup, described in Sec. II, was designed, not only to observe the $\gamma$ rays arising from GDR decay with high efficiency, but also to pin down as precisely as possible the excitation energy and temperature of the hot nuclei through the coincident measurement of evaporation residue velocities and light charged particle spectra and multiplicities. Section III will be devoted to these excitation energy measurements. In Sec. IV the $\gamma$-ray spectra will be presented and their evolution with excitation energy will be discussed. The $\gamma$-ray yield from the GDR will be compared with the predictions of standard statistical model calculations in Sec. V. Section VI contains a comparison of the data with recent theories put forth to explain the saturation of the $\gamma$ yield from the GDR at high excitation energies. Conclusions will be drawn in Sec. VII. Some of the results discussed in this paper have previously been presented [23–30] or published [31].

## II. EXPERIMENTAL METHODS

In order to produce hot nuclei through incomplete fusion reactions, a 300 $\mu$g/cm$^2$ $^{90}$Zr target was bombarded with the 27 MeV/nucleon $^{36}$Ar beam from the GANIL facility, with an average intensity of 10 nA.

Gamma rays and light particles were detected with the MEDEA multidetector [32] (see Fig. 1), which consists of a ball built with 180 barium fluoride ($BaF_2$) crystals, located at 22 cm from the target, which covers the angular range between 30° and 170°, and a solid angle of $3.37\pi$. The crystals are arranged in rings, each ring corresponding to a fixed polar angle $\Theta$ and covering 360° in azimuthal angle $\phi$. The crystals are truncated pyramids 20 cm in length, in order to minimize the cross talk and to optimize the resolu-

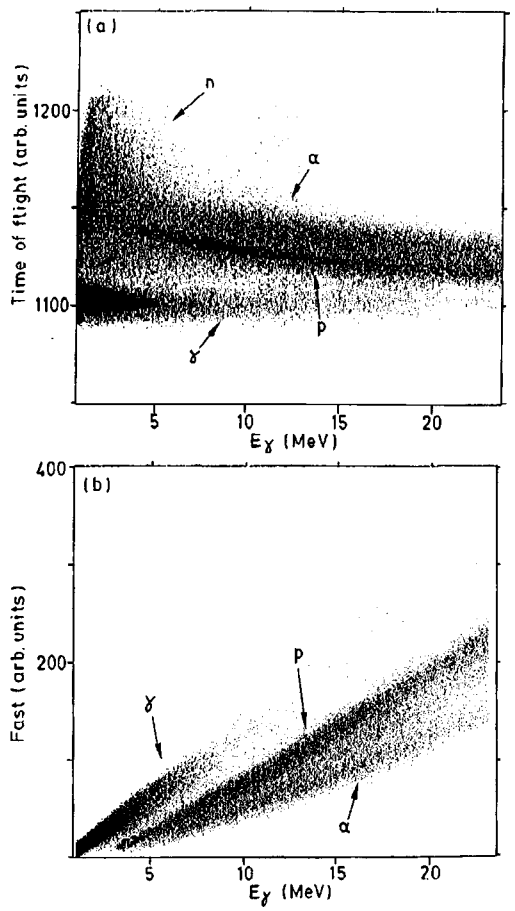


FIG. 2. ''Time of flight'' vs ''total energy'' (a) and ''fast'' vs ''total energy'' (b) scatter plots for a $BaF_2$ detector located in the ring centered at $\Theta = 83°$. The $x$ axis is calibrated in MeV for $\gamma$ rays.

tion for the measurement of high-energy charged particles and $\gamma$ rays. The system is completed by a forward phoswich wall covering the angles between 10° and 30°. To allow for the simultaneous measurement of $\gamma$ rays and light charged particles the entire system operates under vacuum inside a large scattering chamber. The following discussion will be restricted to the results obtained with the $BaF_2$ detectors.

To obtain $\gamma$-ray and particle identification the $BaF_2$ signal is charge integrated during two gates, a fast gate 30 ns long, and a total energy gate, 700 ns long. Moreover, a time of flight measurement, with a resolution of approximately 1 ns, is performed between each $BaF_2$ detector and the cyclotron radio frequency. Figure 2 presents two-dimensional time vs ''total energy'' (a) and ''fast'' vs ''total energy'' (b) scatter plots for a detector in the ring centered at 83°. By applying contours to these planes, an unambiguous separation of $\gamma$ rays from light particles is achieved. Low-energy neutrons (below approximately 20 MeV) give the same pulse shape as $\gamma$ rays [33] and are separated by the time of flight measurement. High-energy neutrons give a pulse shape similar to protons and are separated from the $\gamma$ rays in the ''fast'' vs ''total energy'' plane. However, the contamination of the proton spectra by high-energy neutrons is small due to the low efficiency of the $BaF_2$ detector to such particles [34]. The electronics were adjusted in order to minimize the detection thresholds for light charged particles; however, this

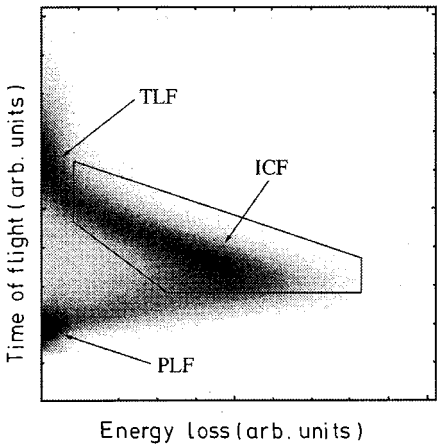


FIG. 3. Two-dimensional energy loss vs time of flight scatter plot for one of the PPAC's. TLF, PLF, and ICF indicate targetlike fragments, projectilelike fragments, and incomplete fusion residues, respectively. The events retained for the analysis are enclosed in the contour line.

setting reduced the quality of the mass identification of $Z = 1$ species, inducing a small deuteron contamination of the proton spectra, mainly at the most forward angles.

The $BaF_2$ detectors were calibrated in energy with the 4.4 and 6.1 MeV gamma rays from AmBe and PuC sources, respectively. These calibrations were checked by measuring cosmic rays [32] and 15.1 MeV $\gamma$ rays from the $^{36}Ar + ^{12}C$ reaction. The light charged particle calibration was deduced from the $\gamma$ calibration using the results of a calibration run performed with light particle beams [35]. In order to take into account the detector response, all the theoretical calculations presented in this paper have been folded with the detector response function, following the methods developed in Ref. [36], which are based on the code EGS3.

Fusionlike residues were detected in two rectangular parallel plate avalanche counters (PPAC's) located in front of the phoswich wall at a distance of 48 cm from the target, covering between 6° and 22° on either side of the beam as shown in Fig. 1. Figure 3 shows a time of flight versus energy loss scatter plot for one of the counters. The start of the time of flight measurement was given by the cyclotron radio frequency. The accumulation at small flight times and low energy losses corresponds to projectilelike fragments which have a velocity close to the beam velocity. The events with low energy losses but long flight times correspond to slow targetlike fragments, probably produced in peripheral collisions. The fusionlike residues exhibit a maximum at large energy losses, prolonged by a tail running towards longer flight times which correspond to more and more incomplete momentum transfers. These fusionlike events, enclosed in the contour in Fig. 3, were retained for the analysis. The events on the rather weakly populated line joining the fusion residues with the projectilelike region are probably due to incompletely relaxed binary collisions (deep-inelastic) and/or fission events, and were not included in the analysis. The time of flight spectrum was calibrated using a time calibrator and the position of the elastic peak which was obtained in a run where the PPAC information was recorded in anticoincidence with the MEDEA ball.

The trigger was given by one PPAC firing in coincidence

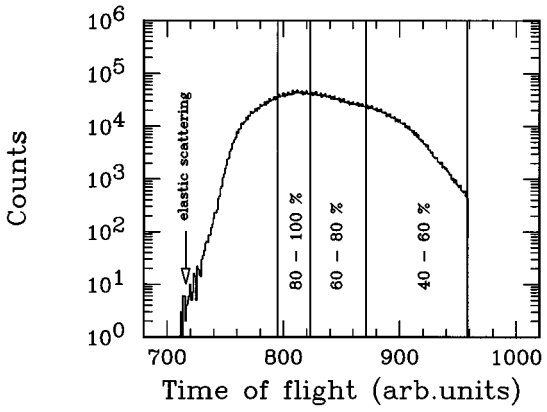


FIG. 4. Time spectrum for one of the PPAC's. The three velocity bins used in the analysis are shown together with the position of the elastic peak determined as described in the text.

with at least one $BaF_2$ detector. This trigger requirement effectively eliminates all cosmic ray contamination of the $\gamma$ spectra. Only those events with at least one $\gamma$ ray with energy greater than 6 MeV were treated in the analysis.

## III. CHARACTERIZATION OF THE HOT NUCLEI

As mentioned previously, at bombarding energies above 10 to 15 MeV/nucleon, incomplete fusion takes over from complete fusion as the main reaction mechanism for central collisions. It thus becomes necessary to characterize the hot nuclei produced in the reaction. This will be attempted here by two methods, the measurement of the velocity of the incomplete fusion residues, from which the initial excitation energies of the nuclei can be deduced through a reaction model, and the measurement of the emitted light particles, which is in principle more model independent.

### A. Residue velocities

A widely used method for characterizing the composite system formed in incomplete fusion reactions is the measurement of the velocity of the evaporation residues. The linear momentum transfer (LMT) [37], the mass of the composite system, and its excitation energy can be deduced from this velocity by applying a massive transfer model [38]. In this simple, but somewhat crude reaction model, part of the light partner, here the projectile, fuses with the target, while the remainder acts as a spectator, and pursues a straight-line trajectory with the velocity of the beam. Moreover, it is assumed that subsequent particle emission is isotropic, and does not modify the average velocity of the recoiling nucleus.

From the time of flight spectrum presented in Fig. 4, we calculate a mean residue velocity of 80% of the center of mass velocity, corresponding to a LMT of about 75% of the full momentum transfer for fusionlike events, which corresponds to an excitation energy of about 560 MeV, and a mass of $A \approx 115$. This is in good agreement with the Viola systematics for momentum transfer as a function of bombarding energy [37].

The time spectrum is broad, showing that a wide range of LMT's, and thus of excitation energies, is populated in the reaction. This is a very attractive feature of intermediate-energy heavy ion reactions since, as long as the hot nuclei produced can be correctly characterized, extended excitation functions can be measured at a single bombarding energy. This property will be used here to follow the evolution of $\gamma$-ray emission as a function of excitation energy. The data have been divided into three bins, depicted in Fig. 4, centered, respectively, at 52%, 69%, and 92% of the center of mass (complete fusion) velocity, and corresponding, according to the massive transfer model, to mean LMT's of 40%, 65%, and 90% of full LMT, to mean initial excitation energies of 360, 480, and 630 MeV, and to initial masses of 105, 113, and 122, respectively.

The massive transfer hypothesis is unfortunately an oversimplified representation of the complex reality of intermediate-energy heavy ion collisions. Even if one considers that the foundation of the model, a substantial mass transfer from projectile to target, is a reasonable starting point to interpret these interactions, two main effects will tend to undermine the reliability of the determination and selection of excitation energies based on this model. First, at this high bombarding energy, preequilibrium particle emission becomes important and is not correctly taken into account, since the massive transfer hypothesis supposes that all nonequilibrium particles are emitted at zero degrees with the beam velocity, which is certainly a poor approximation. Second, a large number of particles are evaporated during the deexcitation of the compound nucleus. This will not affect the mean measured LMT but will tend to smear out the relationship between residue velocity and initial excitation energy. An additional measurement of other observables is necessary to corroborate that the different velocity bins truly correspond to different excitation energies. Here we will analyze the proton spectra in order to extract the temperatures of the hot nuclei.

### B. Proton spectra

For each velocity bin, proton spectra measured in coincidence with evaporation residues were extracted for several angles covering between $69° < \theta_{lab} < 160°$. It was checked that the data reduction condition requiring a $\gamma$ ray with energy above 6 MeV had no influence on the extracted proton spectra. A representative example for the highest velocity bin is given in Fig. 5. The spectra were analyzed in terms of a moving source fit. In incomplete fusion reactions, light particles are usually considered to be of three origins: statistical evaporation from the hot compound nucleus, statistical evaporation from the projectilelike remnant, and fast particles of nonstatistical origin. This nonequilibrium component is generally thought to be due to nucleon-nucleon collisions taking place during the early stages of the reaction [39] and/or to preequilibrium particles emitted by the compound nucleus before thermalization. This contribution is commonly fitted by an intermediate-velocity source exhibiting a high apparent temperature. The projectilelike remnant has a velocity close to the beam velocity and a low temperature and thus will only contribute particles at very forward angles, outside the angular range investigated here. Therefore, only two surface-type Maxwellian sources, a compound nucleuslike (CN) source and an intermediate-velocity (IV) source, were necessary to fit the data over the angular range

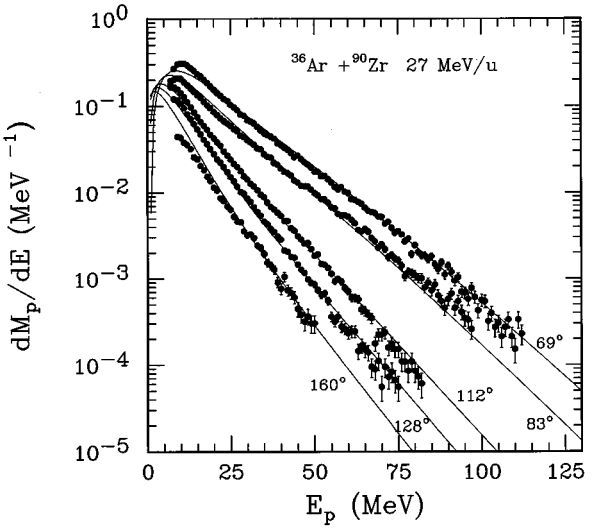


FIG. 5. Proton energy spectra at various angles in coincidence with fusionlike residues from the highest-velocity bin. Solid lines are the result of the fit described in the text.

studied. In the fits the source velocity and temperature and the multiplicity of emitted particles were considered as free parameters. The result of the fit for the highest velocity bin is shown by solid lines in Fig. 5. The relative contributions of the two sources are represented in Fig. 6 for a forward angle and backward angle spectrum. It is interesting to note that even at backward angles the contribution of the IV source is non-negligible for high-energy protons. This shows that the CN temperature cannot simply be inferred from the raw slope of the proton spectra, even measured at the most backward angles.

The extracted parameters of the sources are given in Table I, and are in reasonable agreement with those extracted for similar reactions in Refs. [40,41]. The multiplicity, apparent temperature, and velocity of the compound nucleus source clearly increase between the first two velocity bins, confirming that these two bins correspond to hot nuclei with significantly different temperatures. However, these parameters tend to saturate for the highest residue velocity bin. Such a behavior can be explained by the broadening of the LMT distribution due to evaporation as discussed above. One may also be approaching the limiting temperature that a nucleus can sustain before multifragmentation or vaporization sets in. It can also be noted that the CN source velocities extracted from the moving source fits are in reasonable agreement with the measured residue velocities, underlining the consistency of the analysis. Note that the proton multiplicities for the CN source are much lower than those predicted for such highly excited nuclei by well-established statistical codes such as CASCADE [42] or GEMINI [43], which yield a multiplicity of around 6 at 500 MeV excitation energy. Such low proton multiplicities have already been observed in studies of similar systems [44], and remain hitherto unexplained.

The intermediate source shows a rather different behavior. Its temperature and velocity do not vary significantly, while the multiplicity increases with increasing LMT. This is qualitatively in agreement with a scenario in which these ''pre-equilibrium'' protons are produced by first- and/or low-order nucleon-nucleon collisions and thus their multiplicity reflects the size of the interacting region. Such a behavior has already been observed at higher beam energies [39], and suggests that the highest LMT's come from the most central collisions.

### C. Initial excitation energies and temperatures

The temperature $T_{CN}$ extracted from the moving source fit is a value averaged over the entire decay chain of the hot nucleus. The ratio between this apparent temperature and the initial temperature ($T_{init}$) depends strongly on the type of particle considered. In the literature the value for the ratio $T_{init}/T_{CN}$ is given to be approximately 1.3 in the case of protons for systems in the mass and temperature region studied here [45]. Using this relationship the following initial temperatures were obtained for the three residue velocity bins: 6.0, 6.8, and 7.0 MeV.

The excitation energy is generally inferred from $T_{init}$ through the relationship $E^* = aT^2$ given by the Fermi gas model where $a = A/K$ is the level density parameter. Discounting the highest-velocity bin, the best agreement between the excitation energies deduced from the temperature measurements and those from the velocity measurement is obtained by using $K = 11$ MeV. With this value, an excitation energy of 550 MeV is deduced for the highest-velocity bin, clearly lower than the value given by the massive transfer model. The excitation energies quoted in the following will be 350, 500, and 550 MeV, corresponding to $K = 11$ MeV. This value is in reasonable agreement with recent theoretical calculations [46] which predict an increase of the level den-

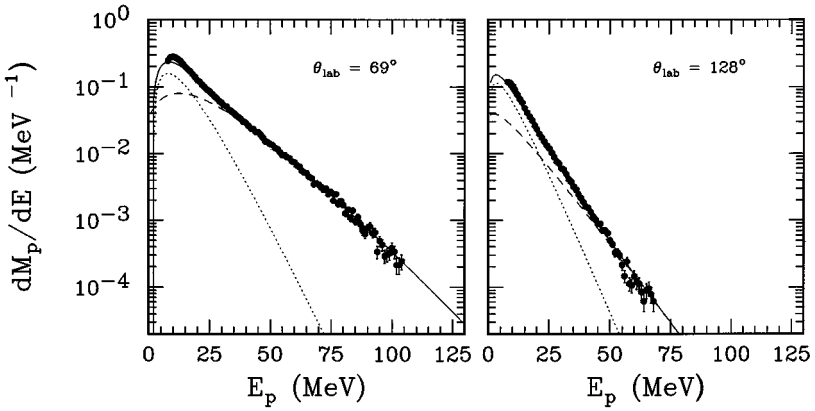


FIG. 6. Proton spectra at two angles in coincidence with fusionlike residues for the highest-velocity bin. Solid lines are the result of the fit with two sources. Dashed and dotted lines are the contributions of the intermediate-velocity source and the compound nucleuslike source, respectively.

TABLE I. Multiplicities, temperatures, and velocities of the two sources extracted from the moving source fits.

| LMT | $M_{CN}$ | $T_{CN}$ (MeV) | $v_{CN}/v_{c.m.}$ | $M_{IV}$ | $T_{IV}$ (MeV) | $v_{IV}/v_{beam}$ |
|---|---|---|---|---|---|---|
| 40% | $1.67 \pm 0.08$ | $4.65 \pm 0.15$ | $0.59 \pm 0.03$ | $1.57 \pm 0.06$ | $9.62 \pm 0.10$ | $0.52 \pm 0.01$ |
| 65% | $1.89 \pm 0.10$ | $5.20 \pm 0.20$ | $0.78 \pm 0.04$ | $2.05 \pm 0.09$ | $9.93 \pm 0.09$ | $0.52 \pm 0.01$ |
| 90% | $2.00 \pm 0.11$ | $5.35 \pm 0.20$ | $0.82 \pm 0.04$ | $2.50 \pm 0.11$ | $10.26 \pm 0.11$ | $0.51 \pm 0.01$ |

sity parameter for Sn nuclei from $K = 8.5$ MeV at zero temperature to $K = 12$ MeV above $T = 5$ MeV, a trend which is corroborated by several experimental studies [44].

Several previous studies of similar systems have yielded comparable values for the excitation energies and temperatures of the hot nuclei formed in incomplete fusion reactions. For the reaction $^{28}Si + ^{100}Mo$ at 25 MeV/nucleon [41], excitation energies between 200 and 400 MeV were extracted depending on momentum transfer. These values are slightly lower than those obtained in the present work but can be understood as due to the lower projectile mass. In the reaction $^{32}S + Ag$ at 30 MeV/nucleon [40], initial compound nucleus temperatures ranging from 6.0 to 6.7 MeV were determined from fits to the $\alpha$-particle spectra, in excellent agreement with the present results obtained from the proton spectra. Note that in this study an estimation of the angular momentum of the hot nuclei was also attempted, and values ranging from $30\hbar$ to $50\hbar$ are reported, depending on residue velocity. In the reaction $^{40}Ar + Ag$ at 27 MeV/nucleon [47] a combination of fits to the proton and $\alpha$-particle spectra yielded initial temperatures between 5.7 and 6.7 MeV, depending on linear momentum transfer, again in remarkable agreement with our analysis.

It is now well established that Boltzmann-Nordheim-Vlasov calculations give a reasonable description of the main features of intermediate-energy heavy ion collisions [48]. It is thus interesting to study the excitation energies predicted by such calculations for the present reaction. The calculations were performed using the code BNV [49]. The calculation was run for several impact parameters between 1 and 7 fm for the reaction $^{36}Ar + ^{90}Zr$ at 27 MeV/nucleon. At 7 fm the excited system fissions but for smaller impact parameters a mechanism akin to incomplete fusion seems to be present, leading to hot nuclei with mean excitation energies of about 450 MeV and mean masses of 120.

The determination of excitation energies reached in the incomplete fusion regime is a demanding task, and the values reported here and in previous work must be considered with rather large error bars. However, two main conclusions can be drawn from the above argumentation, which provide a firm basis for the subsequent analysis of the $\gamma$ spectra. First, the mean excitation energy reached in the reaction studied is about 500 MeV. Second, a clear evolution of the excitation energy is observed between the two lowest-residue-velocity bins, making possible a study of the evolution of the $\gamma$ spectra with increasing temperature, which will be undertaken in the following section.

## IV. GAMMA SPECTRA

### A. Raw $\gamma$ spectra

Figure 7 shows raw $\gamma$ spectra measured at different angles in coincidence with fusionlike residues of the 500 MeV excitation energy bin. These spectra can be qualitatively understood as being composed of three components. At low energies statistical $\gamma$ rays emitted by the compound nucleus at the end of its decay chain give rise to a steep exponential decay. The high-energy photons, above 35 MeV, show an exponentially decaying spectrum. These photons have been interpreted as due to the nucleon-nucleon bremsstrahlung during the initial stages of the collision process [50]. Centered at about 15 MeV, a bump can be seen at all angles, corresponding to $\gamma$ rays from the decay of the GDR excited in nuclei of mass around 115. The spectra at all angles are qualitatively very similar. Slight differences in spectral shapes are due to Doppler shift effects. During the analysis only events containing at least one $\gamma$ ray of energy larger than 6 MeV were considered; therefore, the spectra are displayed only for energies above 6 MeV.

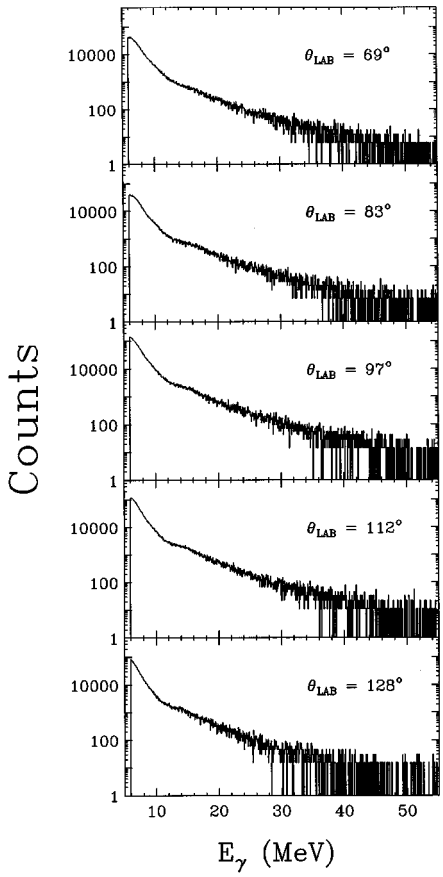


FIG. 7. Raw gamma spectra at various angles in coincidence with fusionlike residues for the excitation energy bin centered at 500 MeV.

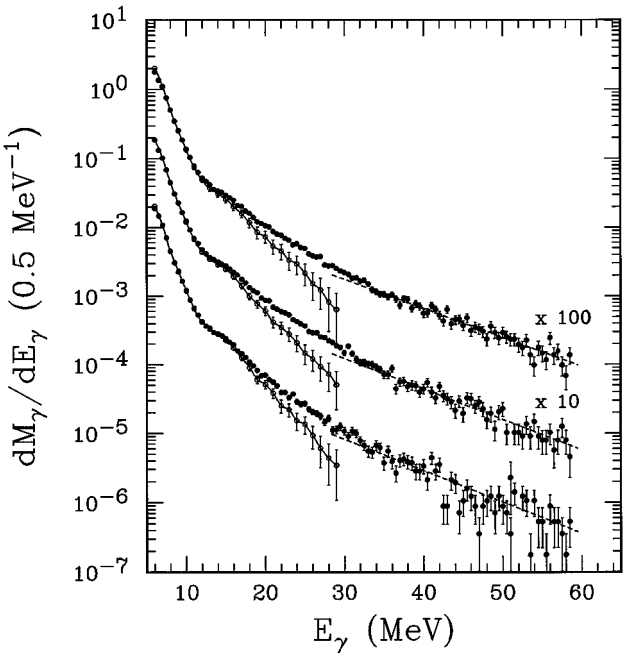


FIG. 8. Solid circles represent the $\gamma$ spectra measured around 90° for the three bins corresponding to mean excitation energies of 550 MeV (top), 500 MeV (middle), and 350 MeV (bottom). The error bars are purely statistical. Dashed lines are the exponential fits for $E_\gamma \geqslant 35$ MeV. Open circles connected by solid lines are the spectra after subtraction of the exponential extrapolated to low energy. In this case the error bars include statistical errors and estimated uncertainties on the exponential fit.

Figure 8 shows the gamma spectra measured in coincidence with fusion events for the three different excitation energy bins. The spectra are summed over the $BaF_2$ detectors of the rings centered at $\theta_{\rm lab}=83°$ and $\theta_{\rm lab}=97°$ where the Doppler shift is negligible. These spectra are presented in units of differential multiplicity, normalized over $4\pi$, i.e., number of $\gamma$ rays per fusionlike residue and per $\gamma$-energy interval. The number of fusionlike residues for each run was deduced from a minimum bias run where only the PPAC triggered the acquisition system, by using the integrated beam current measured in a Faraday cup and taking into account the electronics and computer dead time. The measured differential multiplicities are estimated to be accurate within 10%. This systematic uncertainty is not included in the error bars.

### B. Bremsstrahlung component

In this subsection we will concentrate on the bremsstrahlung component which must be subtracted from the spectra before an analysis of the GDR $\gamma$ yield can be performed. The high-energy $\gamma$ yield can be represented by an exponential function, fitted to the spectrum for $E_\gamma > 35$ MeV. Note that the statistics in the high-energy region is large enough to allow for a precise determination of the slope. The slope parameter for all three bins is $9.5 \pm 1.0$ MeV. This parameter depends essentially on bombarding energy and the value extracted here is in good agreement with the known systematics for nucleon-nucleon bremsstrahlung [50]. Moreover, the high-energy $\gamma$ yield integrated above 35 MeV increases with increasing LMT, as shown in Fig. 9. The solid line corresponds to a constant ratio between the high-energy $\gamma$ yield and the linear momentum transfer and gives an excellent account of the experimental evolution. This evolution can be understood in the framework of a simple geometrical model where the number of nucleon-nucleon collisions is proportional to the overlap volume of the two colliding partners, and thus to the linear momentum transfer. This shows that the hard photon multiplicity is a measure of the impact parameter as already observed at higher bombarding energy [51,52]. The observed evolution of the bremsstrahlung multiplicity confirms that the different residue velocity bins correspond to reactions at different impact parameters as already shown by the proton measurements.

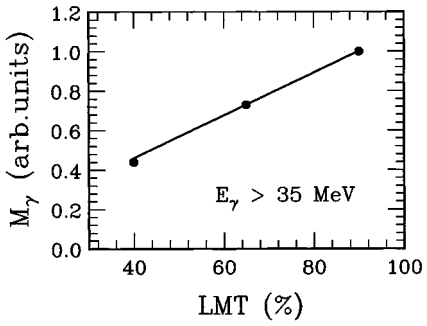


FIG. 9. Multiplicity of hard photons ($E_\gamma \geqslant 35$ MeV) as a function of LMT. The solid line corresponds to a constant ratio between the high-energy $\gamma$ yield and the LMT, and is arbitrarily normalized at the highest LMT.

It should be noted that bremsstrahlung $\gamma$ rays contribute also to the region below 35 MeV, where they no longer dominate the cross section, and thus their contribution is difficult to determine experimentally. In the case of the $^{12}C+^{112,124}Sn$ reactions at 7.5 and 10.5 MeV/nucleon [53] the nonstatistical gamma component has been extracted down to 20 MeV gamma energy and is seen to retain an exponential shape. This experiment was, however, performed at a much lower bombarding energy than ours. From the theoretical point of view, for $^{14}N+^{12}C$ and $^{208}Pb$ reactions at 20, 30, and 40 MeV/nucleon, the bremsstrahlung component down to 20 MeV gamma energy was calculated using the Boltzmann master equation approach [54]. The calculated spectra are seen to retain an approximately exponential shape down to 20 MeV even though a slight increase with respect to an exponential is observed between 20 and 30 MeV. Another calculation, using the molecular dynamics approach, was performed by for light systems at 40 and 84 MeV/nucleon [55]. This calculation shows an approximately exponential shape down to 10 MeV if coherence effects are not taken into account. The inclusion of such effects increases the gamma yield at low energies. From the above considerations it seems that an exponential shape for the bremsstrahlung component is a reasonable approximation at least down to 20 MeV $\gamma$ energy. Therefore, to subtract this component we have chosen to extrapolate the exponential fit down to low energies. Below 20 MeV, the assumption of an exponential is somewhat uncertain. However, here the bremsstrahlung component is small compared to the total cross section, and a variation of its shape would not significantly affect the remaining yield in this region.

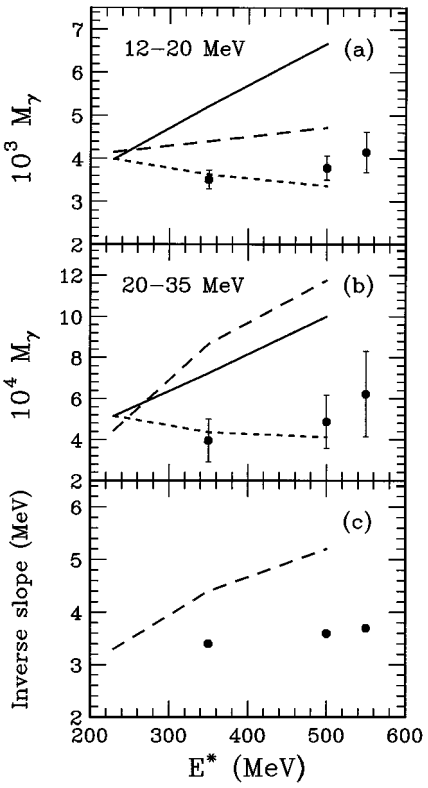


FIG. 10. Calculated and experimental $\gamma$ yields between 12 and 20 MeV (a) and 20 and 35 MeV (b) as a function of excitation energy. Points, experimental results; solid line, standard CASCADE calculation; long-dashed line, CASCADE calculation with increasing GDR width; short-dashed line, CASCADE calculation with cutoff (see text, Sec. VI B). (c) Inverse slope of the $\gamma$ spectra between 20 and 35 MeV after bremsstrahlung subtraction compared to the slope given by the CASCADE calculations with increasing GDR width (see text, Sec. VI B).

In Fig. 8 are shown the spectra for the three LMT bins from which the bremsstrahlung component has been subtracted. The error bars take into account both statistical errors and errors on the slope and normalization of the bremsstrahlung component, encompassing a possible small error on the shape of the component.

### C. Saturation of the $\gamma$ yield from GDR decay

To investigate the evolution of the $\gamma$ decay from the GDR, the $\gamma$ multiplicity was integrated over two regions: from 12 to 20 MeV and 20 to 35 MeV. The first region encompasses the bulk of the GDR $\gamma$ rays but the second is also dominated by the GDR decay. Therefore, to constrain different theoretical interpretations it is important to also investigate the high-energy region of the spectra. The integrated yields are presented in Fig. 10 for the three excitation energy bins. The remarkable feature is that the $\gamma$ yields obtained for the two energy regions increase only very slightly over the excitation energy region populated in the present reaction and can even be considered constant within the error bars. This behavior exhibits a marked change with respect to the evolution of the $\gamma$ yield observed at lower excitation energies, which showed a monotonic increase with excitation energy [6]. This saturation of the GDR $\gamma$ yield at high excitation energies confirms the earlier results obtained for the $^{40}$Ar+$^{92}$Mo reaction at 21 and 26 MeV/nucleon [56], reported for the region between 12 and 20 MeV. It is also in qualitative agreement with the results of Ref. [18] for the $^{40}$Ar+$^{70}$Ge reaction at 15 and 24 MeV/nucleon.

Moreover, the absolute value of the integrated multiplicity in the region between 12 and 20 MeV is about $4\times10^{-3}$ which is in good agreement with the yield reported for the $^{40}$Ar+$^{92}$Mo reaction in Ref. [56]. Chomaz *et al.* [57] predict that the $\gamma$ multiplicity should depend strongly on the dipole moment in the entrance channel. If the two partners exhibit very different $N/Z$ ratios, inducing a large dipole moment in the entrance channel, the GDR will be explicitly excited at the time fusion occurs. These authors thus expect a larger $\gamma$ yield for the present reaction $[(N/Z)_{\rm proj}=1, (N/Z)_{\rm targ}=1.25]$ than for the reaction of Ref. [56] $[(N/Z)_{\rm proj}=1.22, (N/Z)_{\rm targ}=1.19]$. No such effect is observed in the data.

## V. STANDARD STATISTICAL MODEL CALCULATIONS

A large number of factors governs $\gamma$-ray emission. In particular, $\gamma$ rays from GDR decay can be emitted at all steps during the decay chain of the hot nucleus, and therefore the measured $\gamma$ spectrum is not a direct reflexion of the $\gamma$ emission from the compound nucleus at its initial temperature, but rather an average over all temperatures from the initial temperature down to zero. Consequently, a more quantitative analysis of the spectra calls for comparisons with statistical calculations, which take into account the entire decay sequence. Such analyses are generally carried out using the statistical decay code CASCADE [42]. This code treats the statistical emission of $\gamma$ rays, neutrons, protons, and alpha particles from an equilibrated compound nucleus with a given initial excitation energy and angular momentum.

The statistical dipole photon emission rate is given by

$$R_\gamma dE_\gamma = \frac{\rho(E_2)}{\rho(E_1)} f_{\rm GDR}(E_\gamma) dE_\gamma ,$$

where the factor $\rho(E_2)/\rho(E_1)$ is the ratio of the level densities between the final and initial states differing by an energy $E_\gamma = E_1 - E_2$ and $f_{\rm GDR}(E_\gamma) = \sigma_{\rm abs} E_\gamma^3$ is the $E1$ density function which can be written

$$f_{\rm GDR}(E_\gamma) = \frac{4e^2}{3\pi\hbar cmc^2} S_{\rm GDR} \frac{NZ}{A} \frac{\Gamma_{\rm GDR} E_\gamma^4}{(E_\gamma^2 - E_{\rm GDR}^2)^2 + \Gamma_{\rm GDR}^2 E_\gamma^2} .$$

Here $\sigma_{\rm abs}$ represents the photoabsorption cross section and $E_{\rm GDR}$, $\Gamma_{\rm GDR}$, and $S_{\rm GDR}$ are the energy, width, and strength of the GDR, respectively. A Lorentzian line shape is assumed for the GDR, as in the case of cold nuclei measured in photonuclear reactions. Dipole emission is expected to dominate the spectrum but a small contribution from quadrupole decay cannot be *a priori* ruled out. It can be included in the statistical calculation in analogy with the above equation.

The level density parameter is a crucial ingredient in the statistical model calculations. As discussed in Sec. III C this parameter shows a strong temperature dependence and thus cannot be kept constant along the decay chain during the calculation. Reference [46] proposes a parametrization of the

level density parameter for Sn nuclei which varies from $a=A/8.5$ at zero temperature to $a=A/12$ above $T\approx 5$ MeV following

$$a(T)=\frac{(1+0.4e^{-(T/3)^2})}{12}A.$$

This level density parametrization was used in all the calculations. The influence of changes in the level density parameter will be discussed below.

The influence of the initial compound nucleus angular momentum was investigated and seen to be very small as long as it is assumed that the spin does not influence the line shape of the GDR. The determination of the spin distribution for hot nuclei formed in incomplete fusion reactions is not straightforward. We have chosen to perform the calculations for an initial spin of $50\hbar$, close to the value extracted in Ref. [40] for similar reactions. This value is also close to the maximum angular momentum that a Sn nucleus can sustain before fission occurs.

In the following calculations the centroid energy of the GDR is assumed to depend on mass as $E_{\mathrm{GDR}}=76.5A^{-1/3}$ [7]. The sum-rule strength is taken equal to 100% of the TRKSR. The GDR width is kept constant along the decay chain, equal to 12 MeV, which is the saturation value observed in several studies [8,12,13]. The influence of a width increasing with temperature will be investigated in Sec. VI.

We will first evaluate the contribution of quadrupole decay on the spectra. Up to now the giant quadrupole resonance has not been clearly identified built on excited states. For lack of better information, we have considered the contribution of the isoscalar giant quadrupole resonance (ISGQR) and the isovector giant quadrupole resonance (IVGQR) with the parameters reported for these resonances at zero temperature. The parameters of the ISGQR are well known from numerous experiments [1]. For the nuclei considered here, it exhausts 50% of the energy-weighted sum rule (EWSR) at $E_{\mathrm{ISGQR}}=65A^{-1/3}$ MeV with a width of 3.2 MeV. Only scarce experimental results exist for the IVGQR. However, it has been observed in several nuclei with a sum-rule strength varying from 50% to 100% and with an energy that can be parametrized by $E_{\mathrm{IVGQR}}=130A^{-1/3}$ [58,59]. It was included in the calculation with 70% of the EWSR and a width of 8 MeV. Figure 11(a) shows the results of the calculations performed at 500 MeV of excitation energy, with (dashed line) and without (solid line) inclusion of the quadrupole resonances. The ISGQR, located near the same energy as the GDR, contributes only about 1% of the cross section at this energy. The contribution of the IVGQR is small but visible in the region above 20 MeV. However, it can be concluded that the spectrum is dominated by GDR decay and in the following the GQR will no longer be included in the calculations.

In order to compare with the experimental spectra, all the calculated spectra have to be folded with the detector response. This was done following the methods described in Ref. [36] based on the code EGS3. Figure 11(b) shows the spectrum of Fig. 11(a) including only the GDR (solid line) together with the same spectrum folded with the detector response (dashed line).

Figure 12 shows the gamma spectra measured for the 350 and 500 MeV excitation energy bins after subtraction of the bremsstrahlung component. The solid lines correspond to the standard CASCADE calculations described above using the temperature-dependent level density parameter. The low-energy region is rather well reproduced by the calculations. Note that there is no arbitrary normalization involved here. In the region of the GDR the calculations largely overshoot the data. This can be correlated with the observed saturation of the GDR $\gamma$ yield since the calculated yield increases with excitation energy due to the larger number of decay steps in the cascade. The dashed line presented in the 500 MeV case corresponds to a calculation done by using a fixed value $A/10$ of the level density parameter. The use of a constant level density parameter slightly influences the spectral shape but does not modify the above observations. In the following the variable level density parameter will be retained.

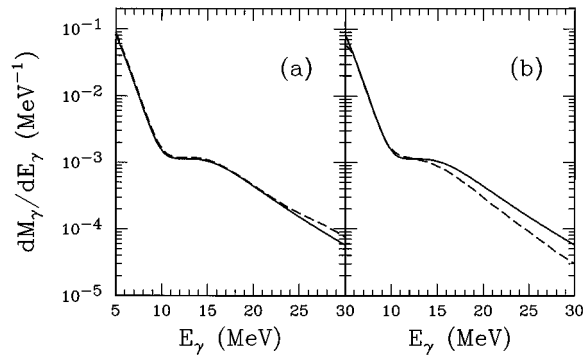


FIG. 11. (a) CASCADE calculations at 500 MeV excitation energy without (solid line) and with (dashed line) inclusion of quadrupole resonances. (b) CASCADE calculations at 500 MeV excitation energy before (solid line) and after (dashed line) folding with the detector response.

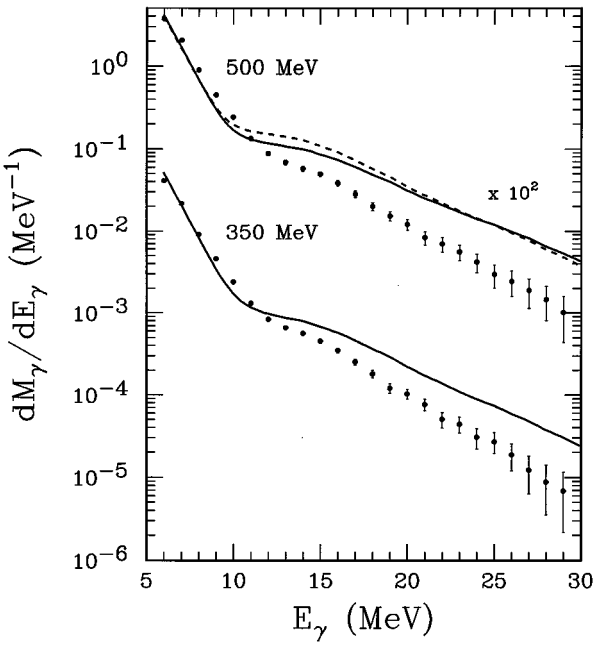


FIG. 12. Gamma spectra for the 350 MeV and 500 MeV excitation energy bins after bremsstrahlung subtraction compared with standard CASCADE calculations (solid lines). In the 500 MeV case the dashed line is a calculation using a constant level density parameter $a=A/10$.

Experimentally, the $\gamma$ yield is observed to saturate as a function of excitation energy in the whole region where the GDR dominates the spectra. Standard statistical calculations cannot reproduce this trend. The elucidation of the mechanism responsible for this quenching could be the key to the understanding of the limits of well-ordered collective motion in nuclei. However, many interwoven effects may play a role in the observed saturation and have generated much theoretical work [17,20–22]. The following section will be devoted to a comparison of theses models with the data.

## VI. THEORETICAL MODELS

### A. Calculations

Theoretical descriptions point to two main effects which can lead to the saturation of the GDR $\gamma$ multiplicity at high excitation energies: a suppression of the GDR at high temperatures [21,22] or a rapid increase of the GDR width with temperature [16,17,20] which leads to a depletion of the gamma yield in the region around 15 MeV since the GDR $\gamma$ rays are spread over a wide energy range.

The model of Bortignon *et al.* [22] takes into account the equilibration time of the GDR with the compound nucleus. At high excitation energies this time is much longer than the particle evaporation time, which precludes the emission of the GDR $\gamma$ rays during the first stages of the decay cascade. In this model the probability for $\gamma$ decay at each step of the cascade is reduced by $\Gamma^{\downarrow}/(\Gamma^{\downarrow}+\Gamma_{ev})$, referred to as the preequilibrium factor, where $\Gamma^{\downarrow}$ is the spreading width of the GDR, and $\Gamma_{ev}$ is the particle evaporation width. Here the ground state spreading width ($\Gamma^{\downarrow}=\Gamma_0=4.8$ MeV) is used, following Ref. [60], according to which the thermal spreading width is temperature independent. The particle evaporation width increases rapidly as a function of excitation energy, leading to a suppression of GDR gamma emission at the highest temperatures as shown by the solid line in Fig. 13.

Chomaz [21] proposes that the quenching of the GDR strength is related to the fact that each individual particle emission induces a strong fluctuation of the dipole moment of the nucleus. When the temperature increases the time between two particle emissions becomes shorter than the characteristic GDR vibration time. In such a case the motion is no longer characterized by the GDR frequency and the observed $\gamma$ spectrum will be flat. This argument leads to a reduction factor given by $\exp(-2\pi\Gamma_{ev}/E_{GDR})$ which is shown by a dashed line in Fig. 13. The reduction predicted by this model has a similar energy dependence as for the preequilibrium model, but is much stronger.

Smerzi *et al.* [16,17] predict a strong increase of the GDR spreading width with excitation energy due to the damping through two-body collisions. This width can be parametrized for all excitation energies by $\Gamma_{GDR}=\Gamma_0+0.0026(E^*)^{1.6}$, in agreement with the experimental systematics of [61,62] below 130 MeV excitation energy, but rising much faster above. This evolution is shown by a dot-dashed line in Fig. 14. In this calculation the preequilibrium factor discussed in the first case was also included. However, here the spreading width of the GDR ($\Gamma^{\downarrow}$) in this factor is temperature dependent and given by the above parametrization and therefore its effect is smaller as shown by the dot-dashed line in Fig. 13.

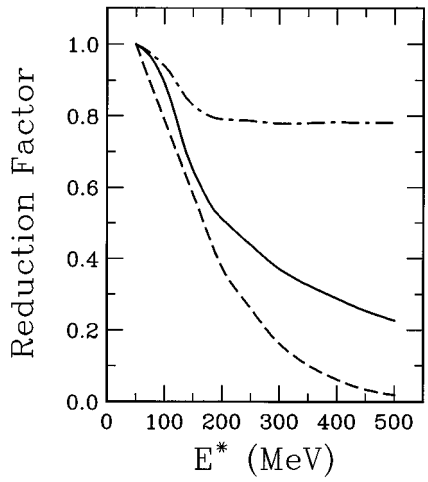


FIG. 13. Reduction factor predicted by the models of Bortignon *et al.* [22] (solid line), Chomaz [21] (dashed line), and Smerzi *et al.* [17] (dot-dashed line) as a function of excitation energy.

The reduction of the GDR $\gamma$ yield is mainly due to the large increase of the width of the GDR rather than to preequilibrium effects.

In another model, Chomaz [20] points out that, since the observed GDR photons are coming from transitions between two states of the compound nucleus which have finite lifetimes, the measured GDR width must contain the widths of the initial and final states. This leads to a rapid increase of the measured GDR width with temperature, as depicted by a dotted line in Fig. 14.

We have performed complete CASCADE calculations incorporating the prescriptions of these different models. The results of these calculations for 500 MeV excitation energy are shown in the top part of Fig. 15.

The solid line shows the calculation following the preequilibrium model of Ref. [22]. In this calculation, the total width of the GDR was chosen to follow the experimental evolution compiled in [61,62], i.e., parametrized by $\Gamma_{GDR}=4.8+0.0026(E^*)^{1.6}$ MeV below 130 MeV excitation

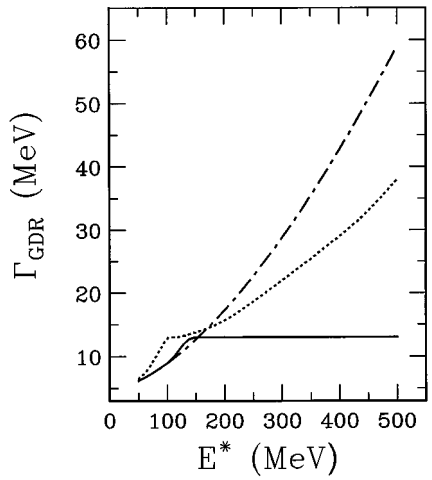


FIG. 14. Evolution of the width of the GDR with excitation energy as predicted by the models of Chomaz [20] (dotted line) and Smerzi *et al.* [17] (dot-dashed line). The solid line represents the experimental systematics of Refs. [61,62].

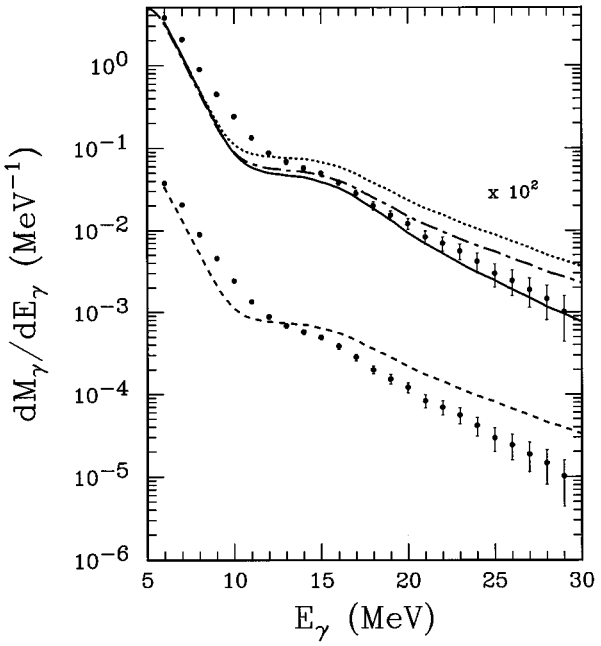


FIG. 15. Top: gamma spectrum for the 500 MeV excitation energy bin after bremsstrahlung subtraction, compared with CASCADE calculation including the theoretical prescriptions of Bortignon *et al.* [22] (solid line), Chomaz [20] (dotted line), and Smerzi *et al.* [17] (dot-dashed line) (see text). Bottom: same spectrum compared to a CASCADE calculation (dashed line) with $\Gamma_{\mathrm{GDR}}=4.8+0.0026(E^*)^{1.6}$ MeV.

energy and saturated at 12 MeV above 130 MeV. In the region near the centroid of the GDR the yield is largely reduced with respect to the standard CASCADE calculation and even falls somewhat below the experimental points. The data are well reproduced in the high-energy region but markedly underestimated between 8 and 12 MeV.

A calculation incorporating the reduction factor proposed by Chomaz [21] and using the same hypothesis as above for the width of the GDR was also performed. The resulting spectrum falls far below the experimental results in the entire GDR region and is not shown.

The result of the calculation following the collisional damping model of Refs. [16,17], which predicts a strongly increasing GDR width, is presented by a dot-dashed line in Fig. 15. The yield is well reproduced in the region of the centroid of the GDR but largely overestimated at higher energies. One may wonder if this overestimation could be due to an error on the slope or the normalization of the subtracted bremsstrahlung component. Recall, however, that the error bars of the spectrum include uncertainties on the bremsstrahlung subtraction. Only the assumption of a complete absence of the bremsstrahlung component, which would be in contradiction with all known systematics, could lead to agreement between the data and the calculations in this high-energy region. Again the yield is underestimated between 8 and 12 MeV.

Finally, the dotted line shows the prediction of the model taking into account the widths of the initial and final states of the $\gamma$ decay [20]. The result is very similar to that of the previous calculation with a slightly larger overestimation of the data in the high-energy region.

### B. Discussion

Let us first consider the case of the continuously increasing GDR width. Both models which incorporate such an effect indeed lead to a decrease of the GDR $\gamma$ yield near the centroid of the resonance. However, this is achieved at the expense of of a marked overestimation of the data at higher energies. To study this effect we have performed for several excitation energies supplementary calculations without including any particular model, simply using a continuously increasing width $\Gamma_{\mathrm{GDR}}=4.8+0.0026(E^*)^{1.6}$ MeV [61] (dot-dashed line in Fig. 14). The result of this calculation for 500 MeV excitation energy, shown by a dashed line in the bottom part of Fig. 15, is close to those obtained by using models including a continuously increasing width. The integrated $\gamma$ multiplicities for energy regions from 12 to 20 MeV and from 20 to 35 MeV are compared to the experimental data in Figs. 10(a) and 10(b), respectively. For reference the yields for the standard CASCADE calculations are also reported in this figure. The calculated yield in the 12–20 MeV region lies slightly above the data but shows the same flat evolution with excitation energy. This is no longer the case in the region between 20 and 35 MeV where the calculated yield increases strongly with excitation energy, even faster that the standard CASCADE calculation. Furthermore, the slope of the calculated spectrum above 20 MeV increases with excitation energy in contradiction with the experimental slope as can be seen in Fig. 10(c). This effect is simply understood from the statistical dipole photon emission rate given in Sec. V. In this equation the ratio of level densities $\rho(E_2)/\rho(E_1)$ is roughly proportional to $e^{-E_\gamma/T}$. With increasing temperature this factor tends to increase the $\gamma$ multiplicity at higher energies by decreasing the slope of the spectrum. Moreover, the Lorentzian representing the GDR strength function is multiplied by $E_\gamma^3$ which shifts the $\gamma$ yield to higher energies when the GDR width increases. Therefore the above conclusions can be generalized to all calculations which attempt to interpret the quenching of the GDR $\gamma$ yield in terms of a continuously increasing width of the GDR with temperature. In conclusion the GDR $\gamma$ emission must be hindered by another mechanism than an increase of the width.

The proposal of Bortignon *et al.* [22], to take into account the equilibration time of the GDR with the compound nucleus, discussed in the previous subsection, gives a reasonable account of the data (see Fig. 15). This model predicts a smooth cutoff of the $\gamma$ emission, as shown in Fig. 13. A hypothesis of this model is that no giant dipole resonance is present at the time of formation of the compound nucleus. Such a hypothesis is probably reasonable if the projectile and target have the same $N/Z$ ratio. However, in the present case the $N/Z$ ratios of the two partners are quite different and a substantial dipole moment is present in the entrance channel. One thus expects the presence of GDR phonons already in the very early stage of the reaction, before equilibration is achieved [21]. If these phonons have the same energy as the GDR of the equilibrated compound nucleus, their $\gamma$ decay would populate the region of the GDR in the spectra. This would cast some doubt on the possibility to consistently apply this model to our data. However, it will be discussed below that the fusing system may be deformed and thus the dipole phonons could be shifted to lower energy [63].

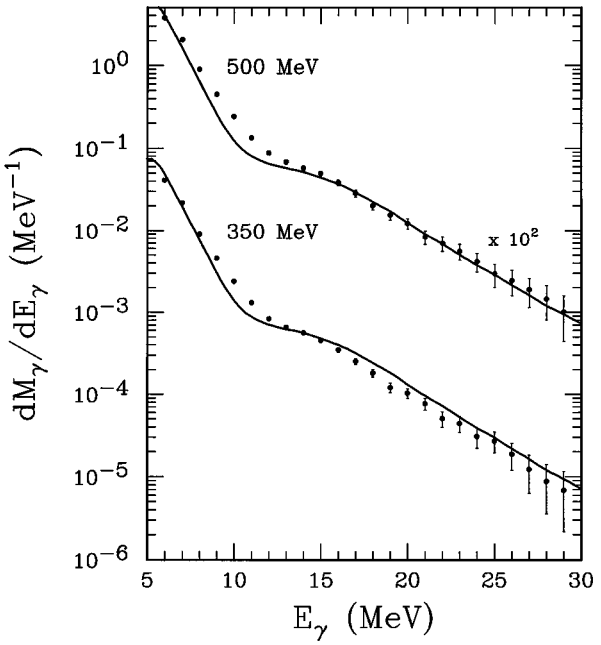


FIG. 16. Gamma spectra for the 350 and 500 MeV excitation energy bins after bremsstrahlung subtraction, compared with CASCADE calculations including a cutoff of gamma emission above 250 MeV.

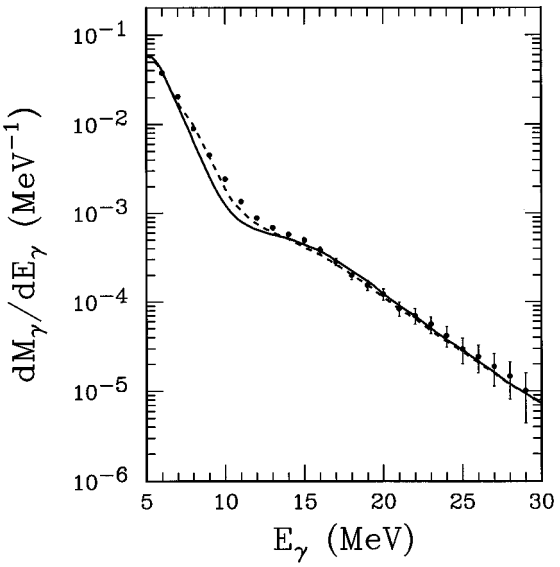


FIG. 17. Gamma spectrum for the 500 MeV excitation energy bin after bremsstrahlung subtraction, compared with the CASCADE calculation of Fig. 16 (solid line) and a CASCADE calculation with dipole strength centered around 8 MeV above 200 MeV excitation energy (dashed line; see text).

The simplest way to simulate the complete $\gamma$ spectrum above 12 MeV is to introduce a sharp suppression of the $\gamma$ emission above a given excitation energy. Such a calculation using a constant width of 12 MeV for the GDR, and a cutoff excitation energy of 250 MeV allows one to reproduce the $\gamma$ spectra above 12 MeV measured for the all three excitation energy bins, as shown in Fig. 16 for the 350 and 500 MeV bins. The integrated yields and the slope parameters are also plotted in Fig. 10, in good agreement with the data. Note that the precise shape of the cutoff cannot be inferred from the present data and different types of smooth cutoffs could also reproduce the spectra.

An intriguing feature of the data is that all the calculations underestimate the $\gamma$ yield between 8 and 12 MeV. Note also that a similar trend can be found in the results of Gaardhøje *et al.* [18] and also at much lower excitation energies as pointed out by Thoennessen [64] in a comment on the work of Morsch *et al.* [65] and further discussed in the reply of Morsch *et al.* [66] to the comment. Such low-energy strength can also be seen in the study of Chakrabarty *et al.* [61], where it is attributed to an artifact due to the incomplete subtraction of slow neutron capture events in the NaI crystals. The experiments of Refs. [18,65] were also performed with NaI detectors; however, it is not clear if or how these neutron capture events were subtracted.

The present measurements were done with BaF2 detectors, which do not present the same effect for neutron capture. Moreover, a possible contamination of the $\gamma$ spectra in this region by misidentified fast neutrons is ruled out by the fact that the spectra corrected for the Doppler shift are identical at all angles. One would expect a much larger contamination from fast neutrons at forward angles.

A possible explanation for the excess strength observed here could be that the GDR is replaced by some strength around 8 MeV as one approaches very high excitation energies. This tendency can be found in several random phase approximation calculations at high temperatures [63,67,68]. In a crude attempt to ascertain if such a hypothesis is compatible with the data we have performed CASCADE calculations in which the GDR is replaced by a low-lying component above a certain excitation energy. Figure 17 shows the result of a calculation where the $E1$ strength with a Lorentzian shape of centroid 8 MeV and width 4 MeV exhausting 50% of the TRKSR is assumed to be present above 200 MeV excitation energy. Below 200 MeV the standard GDR parameters are used ($E_{\mathrm{GDR}} = 76.5A^{-1/3}$, $\Gamma_{\mathrm{GDR}} = 12$ MeV, and $S_{\mathrm{GDR}} = 100\%$ TRKSR). Indeed, such a calculation exhibits a very good reproduction of the data, giving the correct order of magnitude for the yield between 8 and 12 MeV. The hypothesis of the existence of low-lying strength could be a reasonable interpretation of the observed excess yield. However, reality is bound to be more complex than the crude parametrization used here, and theoretical strength functions as a function of temperature, which could be included in a CASCADE calculation, would be necessary to extract more precise information on the evolution of the dipole strength with temperature.

Another possibility to explain the excess low-energy yield could be the emission of preequilibrium $\gamma$ rays due to the presence of a strong dipole moment in the entrance channel of the reaction studied. Boltzmann-Nordheim-Vlasov calculations were performed by Bortignon *et al.* [63], and the Fourier transform of the dipole moment, calculated up to equilibration time, shows main frequencies much lower than the one obtained for the GDR in the compound nucleus. This is understood in terms of the large deformation of the fusing system in the entrance channel. Therefore $\gamma$ rays emitted before equilibration may well populate the region of the spectrum below 12 MeV, where an excess yield is measured.

This effect may also help justify the use of the model of Ref. [22].

## VII. CONCLUSIONS

Hot nuclei formed in the $^{36}Ar+^{90}Zr$ reaction at 27 MeV/nucleon were studied through the simultaneous measurement of the emitted $\gamma$ rays, light charged particles, and evaporation residues using the MEDEA detector installed at the GANIL facility. The emphasis of this work was placed on the study of the giant dipole resonance excited in these hot nuclei, in order to follow the properties of collective motion as one approaches the limiting temperatures that nuclei can sustain.

The excitation energies and temperatures of the nuclei were inferred from the measurement of the evaporation residue velocities by applying a massive transfer model, and through moving source fits to the coincident proton spectra. A coherent picture emerges, showing that the hot nuclei produced with mass around 115 exhibit a range of excitation energies between 350 and 550 MeV, corresponding to initial temperatures of 6–7 MeV, in agreement with previous studies of similar systems. This allows one to study the evolution of the GDR parameters as a function of excitation energy, using a single bombarding energy.

The GDR is measured through its $\gamma$ decay and shows up as a prominent bump located around 15 MeV in the coincident $\gamma$ spectra, which subsists up to the highest excitation energies reached. In the region between 12 and 20 MeV, which contains the bulk of the GDR $\gamma$ rays, the integrated $\gamma$ multiplicity, after bremsstrahlung subtraction, is constant (about $4\times10^{-3}$) as a function of excitation energy. This value is close to the saturation value reported for the $^{40}Ar+^{92}Mo$ reaction in Ref. [56]. Therefore, no effect is observed due to the different entrance channel dipole moments arising from different $N/Z$ asymmetries between projectile and target of these two reactions. The region of the spectra between 20 and 35 MeV is also dominated by GDR decay, and here also the integrated yield shows a saturation as a function of excitation energy. Standard statistical model calculations using the code CASCADE, assuming a saturation of the GDR width and full sum-rule strength, which reproduced earlier experimental results up to 230 MeV excitation energy, strongly overshoot the spectra measured here, and fail to reproduce the observed saturation.

To explain the saturation of the GDR $\gamma$ multiplicity several theoretical models have been proposed. CASCADE calculations were performed including the prescriptions of these models. All the models which predict a continuous increase of the width of the GDR with temperature [17,21] yield a saturation of the $\gamma$ multiplicity between 12 and 20 MeV, but at the expense of a strong increase of the yield above 20 MeV, which is at variance with the experimental observations. On the contrary the experimental data seem to be in agreement with a simple prescription where no GDR $\gamma$ rays are emitted above 250 MeV excitation energy. If no dipole moment is present in the entrance channel, a similar cutoff is predicted by taking into account the equilibration time of the GDR with the compound nucleus [22]. This is, however, not the case of the present experiment. A transition from coherent to chaotic motion for the GDR in the excitation energy range studied would also suppress GDR decay during the first steps of the evaporation chain [21].

Between 8 and 12 MeV all the model calculations underestimate the measured yield. The excess yield could be compatible with the appearance of a low-lying component of $E1$ strength at high temperatures, as predicted by several RPA calculations. More experimental and theoretical work is necessary to confirm this intriguing possibility.

This work has demonstrated the existence of a limiting excitation energy for the observation of the GDR in nuclei through its $\gamma$ decay, which is clearly lower than the limiting excitation energy for the existence of nuclei. This limit may signal a transition towards chaotic motion in highly excited nuclei or could be a fingerprint of the shift towards lower energies of the dipole strength at very high temperatures. The elucidation of this question should be the aim of future experiments.

## ACKNOWLEDGMENTS

We warmly thank P.F. Bortignon and M. Di Toro for numerous fruitful discussions. The help of A. Peghaire during the experiment is gratefully acknowledged. We thank R. Berthelot, A. Di Stefano, and P. Lelong for their technical help during the setting up of the experiment. This experiment was performed at the GANIL national facility, Caen, France.

[1] A. van der Woude, Prog. Part. Nucl. Phys. **18**, 217 (1987).
[2] D. M. Brink, Ph.D. thesis, University of Oxford, 1955.
[3] M. A. Kovash, S. L. Blatt, R. N. Boyd, T. R. Donoghue, H. J. Hausman, and A. D. Bacher, Phys. Rev. Lett. **42**, 700 (1979).
[4] D. H. Dowell, G. Feldman, K. A. Snover, A. M. Sandorfi, and M. T. Collins, Phys. Rev. Lett. **50**, 1191 (1983).
[5] K. A. Snover, Annu. Rev. Nucl. Part. Sci. **36**, 586 (1986).
[6] J. J. Gaardhøje, Annu. Rev. Nucl. Part. Sci. **42**, 483 (1992).
[7] B. L. Berman and S. C. Fultz, Rev. Mod. Phys. **47**, 713 (1975).
[8] A. Bracco, J. J. Gaardhøje, A. M. Bruce, J. D. Garrett, B. Herskind, M. Pignanelli, D. Barnéoud, H. Nifenecker, J. A. Pinston, C. Ristori, F. Schussler, J. Bacelar, and H. Hofmann, Phys. Rev. Lett. **62**, 2080 (1989).
[9] A. Bracco, F. Camera, M. Mattiuzzi, B. Million, M. Pignanelli, J. J. Gaardhøje, A. Maj, T. Ramsøy, T. Tveter, and Z. Zelazny, Phys. Rev. Lett. **74**, 3748 (1995).
[10] E. Ramakrishnan, T. Baumann, A. Azhari, R. A. Kryger, R. Pfaff, M. Thoennessen, S. Yokoyama, J. R. Beene, M. L. Halbert, P. E. Mueller, D. W. Stracener, R. L. Varner, R. J. Charity, J. F. Dempsey, D. G. Sarantites, and L. G. Sobotka, Phys. Rev. Lett. **76**, 2025 (1996).
[11] D. Pierroutsakou, Ph.D. thesis, Orsay, France, 1993; D. Pierroutsakou *et al.*, Nucl. Phys. A (to be published).
[12] H. J. Hofmann, J. C. Bacelar, M. N. Harakeh, T. D. Poelhekken, and A. van der Woude, Nucl. Phys. **A571**, 301 (1994).
[13] G. Enders, F. D. Berg, K. Hagel, W. Kühn, V. Metag, R. Novotny, M. Pfeiffer, O. Schwalb, R. J. Charity, A. Gobbi, R. Freifelder, W. Henning, K. D. Hildenbrand, R. Holtzman, R.

S. Mayer, R. S. Simon, J. P. Wessels, G. Casini, A. Olmi, and A. A. Stefanini, Phys. Rev. Lett. **69**, 249 (1992).

[14] K. Yoshida, J. Kasagi, H. Hama, M. Sakurai, M. Kodama, K. Furutaka, K. Ieki, W. Galster, T. Kubo, and M. Ishihara, Phys. Lett. B **245**, 7 (1990).

[15] J. Kasagi, K. Furutaka, T. Murakami, A. Yajima, M. Oshima, S. Niiya, H. Tominaga, K. Yoshida, H. Hama, K. Ieki, W. Galster, K. Kubo, M. Ishihara, and A. Galonsky, Nucl. Phys. **A538**, 585c (1992).

[16] A. Smerzi, A. Bonasera, and M. Di Toro, Phys. Rev. C **44**, 1713 (1991).

[17] A. Smerzi, M. Di Toro, and D. M. Brink, Phys. Lett. B **320**, 216 (1994).

[18] J. J. Gaardhøje, A. M. Bruce, J. D. Garrett, B. Herskind, M. Maurel, H. Nifenecker, J. A. Pinston, P. Perrin, C. Ristori, F. Schussler, A. Bracco, and M. Pignanelli, Phys. Rev. Lett. **59**, 1409 (1987).

[19] J. Kasagi and K. Yoshida, Nucl. Phys. **A569**, 195c (1994).

[20] Ph. Chomaz, Phys. Lett. B **347**, 1 (1995).

[21] Ph. Chomaz, Nucl. Phys. **A569**, 203c (1994).

[22] P. F. Bortignon, A. Bracco, D. Brink, and R. A. Broglia, Phys. Rev. Lett. **67**, 3360 (1991).

[23] T. Suomijärvi, J. H. Le Faou, Y. Blumenfeld, P. Piattelli, C. Agodi, N. Alamanos, R. Alba, F. Auger, G. Bellia, Ph. Chomaz, R. Coniglione, A. Del Zoppo, P. Finocchiaro, N. Frascaria, J. J. Gaardhoje, J. P. Garron, A. Gillibert, M. Lamehi-Rachti, R. Liguori-Neto, C. Maiolino, E. Migneco, G. Russo, J. C. Roynette, D. Santonocito, P. Sapienza, J. A. Scarpaci, and A. Smerzi, in *Proceedings of the 1st Joint Italian-Japanese Meeting on Perspectives in Heavy Ion Physics*, edited by M. Di Toro and E. Migneco (Editrice Compositori, Bologna, 1993), p. 189.

[24] J. H. Le Faou, T. Suomijärvi, Y. Blumenfeld, P. Piattelli, C. Agodi, N. Alamanos, R. Alba, F. Auger, G. Bellia, Ph. Chomaz, R. Coniglione, A. Del Zoppo, P. Finocchiaro, N. Frascaria, J. J. Gaardhoje, J. P. Garron, A. Gillibert, M. Lamehi-Rachti, R. Liguori-Neto, C. Maiolino, E. Migneco, G. Russo, J. C. Roynette, D. Santonocito, P. Sapienza, J. A. Scarpaci, and A. Smerzi, in Proceedings of the XXXI International Winter Meeting on Nuclear Physics, Bormio, Italy, 1993, edited by I. Iori (unpublished), p. 417.

[25] Y. Blumenfeld, J. H. Le Faou, T. Suomijärvi, P. Piattelli, C. Agodi, N. Alamanos, R. Alba, F. Auger, G. Bellia, Ph. Chomaz, R. Coniglione, A. Del Zoppo, P. Finocchiaro, N. Frascaria, J. J. Gaardhoje, J. P. Garron, A. Gillibert, M. Lamehi-Rachti, R. Liguori-Neto, C. Maiolino, E. Migneco, G. Russo, J. C. Roynette, D. Santonocito, P. Sapienza, J. A. Scarpaci, and A. Smerzi, in Proceedings of the International School-Seminar on Heavy ion Physics, Dubna, Russia, 1993, edited by Yu. Ts. Oganessian, Yu. E. Penionzhkevich, and R. Kalpakchieva (unpublished), Vol. 1, p. 466.

[26] T. Suomijärvi, J. H. Le Faou, Y. Blumenfeld, P. Piattelli, C. Agodi, N. Alamanos, R. Alba, F. Auger, G. Bellia, Ph. Chomaz, R. Coniglione, A. Del Zoppo, P. Finocchiaro, N. Frascaria, J. J. Gaardhoje, J. P. Garron, A. Gillibert, M. Lamehi-Rachti, R. Liguori-Neto, C. Maiolino, E. Migneco, G. Russo, J. C. Roynette, D. Santonocito, P. Sapienza, J. A. Scarpaci, and A. Smerzi, Nucl. Phys. **A569**, 225c (1994).

[27] Y. Blumenfeld, J. H. Le Faou, T. Suomijärvi, P. Piattelli, C. Agodi, N. Alamanos, R. Alba, F. Auger, G. Bellia, Ph. Chomaz, R. Coniglione, A. Del Zoppo, P. Finocchiaro, N. Frascaria, J. J. Gaardhoje, J. P. Garron, A. Gillibert, M. Lamehi-Rachti, R. Liguori-Neto, C. Maiolino, E. Migneco, G. Russo, J. C. Roynette, D. Santonocito, P. Sapienza, J. A. Scarpaci, and A. Smerzi, in Proceedings of the XXXII International Winter Meeting on Nuclear Physics, Bormio, Italy, 1994, edited by I. Iori (unpublished), p. 267.

[28] P. Piattelli, J. H. Le Faou, T. Suomijärvi, Y. Blumenfeld, C. Agodi, N. Alamanos, R. Alba, F. Auger, G. Bellia, Ph. Chomaz, R. Coniglione, A. Del Zoppo, P. Finocchiaro, N. Frascaria, J. J. Gaardhoje, J. P. Garron, A. Gillibert, M. Lamehi-Rachti, R. Liguori-Neto, C. Maiolino, E. Migneco, G. Russo, J. C. Roynette, D. Santonocito, P. Sapienza, J. A. Scarpaci, and A. Smerzi, in Proceedings of the 3rd Course of the International School of Heavy Ion Physics, Erice, Italy, 1994, edited by R. A. Broglia, P. Kienle, and P. F. Bortignon (unpublished), p. 298.

[29] T. Suomijärvi, J. H. Le Faou, Y. Blumenfeld, P. Piattelli, C. Agodi, N. Alamanos, R. Alba, F. Auger, G. Bellia, Ph. Chomaz, R. Coniglione, A. Del Zoppo, P. Finocchiaro, N. Frascaria, J. J. Gaardhoje, J. P. Garron, A. Gillibert, M. Lamehi-Rachti, R. Liguori-Neto, K. Loukachine, C. Maiolino, E. Migneco, S. Montironi, G. Russo, J. C. Roynette, D. Santonocito, P. Sapienza, J. A. Scarpaci, and A. Smerzi, Nucl. Phys. **A583**, 105c (1995).

[30] J. H. Le Faou, Ph.D. thesis, Internal Report No. IPNO-T-94-01, Université Paris-Sud, 1994.

[31] J. H. Le Faou, T. Suomijärvi, Y. Blumenfeld, P. Piattelli, C. Agodi, N. Alamanos, R. Alba, F. Auger, G. Bellia, Ph. Chomaz, R. Coniglione, A. Del Zoppo, P. Finocchiaro, N. Frascaria, J. J. Gaardhoje, J. P. Garron, A. Gillibert, M. Lamehi-Rachti, R. Liguori-Neto, C. Maiolino, E. Migneco, G. Russo, J. C. Roynette, D. Santonocito, P. Sapienza, J. A. Scarpaci, and A. Smerzi, Phys. Rev. Lett. **72**, 3321 (1994).

[32] E. Migneco, C. Agodi, R. Alba, G. Bellia, R. Coniglione, A. Del Zoppo, P. Finocchiaro, C. Maiolino, P. Piattelli, G. Raia, and P. Sapienza, Nucl. Instrum. Methods Phys. Res. A **314**, 31 (1992).

[33] T. Matulewicz, E. Grosse, H. Emling, H. Grein, R. Kulessa, F. M. Baumann, G. Domogala, and H. Freiesleben, Nucl. Instrum. Methods Phys. Res. A **274**, 501 (1989).

[34] S. Kubota, T. Motobayashi, M. Ogiwara, H. Murakami, Y. Ando, J. Ruan, S. Shirato, and T. Murakami, Nucl. Instrum. Methods Phys. Res. A **285**, 436 (1989).

[35] A. Del Zoppo, C. Agodi, R. Alba, G. Bellia, R. Coniglione, P. Finocchiaro, C. Maiolino, E. Migneco, A. Peghaire, P. Piattelli, and P. Sapienza, Nucl. Instrum. Methods Phys. Res. A **327**, 363 (1993).

[36] G. Bellia, R. Alba, R. Coniglione, A. Del Zoppo, P. Finocchiaro, C. Maiolino, E. Migneco, P. Piattelli, P. Sapienza, N. Frascaria, I. Lhenry, J. C. Roynette, T. Suomijärvi, N. Alamanos, F. Auger, A. Gillibert, D. Pierroutsakou, J. L. Sida, and P. R. Silveira Gomes, Nucl. Instrum. Methods Phys. Res. A **329**, 173 (1993).

[37] V. E. Viola, Jr., B. B. Back, K. L. Wolf, T. C. Awes, C. K. Gelbke, and H. Breuer, Phys. Rev. C **26**, 178 (1982).

[38] H. Nifenecker, J. Blachot, J. Crançon, A. Gizon, and A. Lleres, Nucl. Phys. **A447**, 533c (1985).

[39] R. Alba, R. Coniglione, A. del Zoppo, C. Agodi, G. Bellia, P. Finocchiaro, K. Loukachine, C. Maiolino, E. Migneco, P. Piattelli, D. Santonocito, P. Sapienza, A. Peghaire, I. Iori, L. Manduci, and A. Moroni, Phys. Lett. B **322**, 38 (1994).

[40] R. Wada, D. Fabris, G. Nebbia, Y. Lou, M. Gonin, J. B. Natowitz, R. Billerey, B. Cheynis, A. Demeyer, D. Drain, D. Guinet, C. Pastor, J. Alarja, A. Giorni, D. Heuer, C. Morand, J. B. Viano, C. Mazur, C. Ngô, S. Leray, R. Lucas, M. Ribrag, and E. Tomasi, Phys. Rev. C **39**, 497 (1989).

[41] A. Chbihi, L. G. Sobotka, Z. Majka, D. G. Sarantites, D. W. Stracener, V. Abenante, T. M. Semkow, N. G. Nicolis, D. C. Hensley, J. R. Beene, and M. L. Halbert, Phys. Rev. C **34**, 652 (1991).

[42] F. Pühlhofer, Nucl. Phys. **A280**, 267 (1977).

[43] R. J. Charity, D. R. Bowman, Z. H. Liu, R. J. McDonald, M. A. McMahan, G. J. Wozniak, L. G. Moretto, S. Bradley, W. L. Kehoe, and A. C. Mignerey, Nucl. Phys. **A476**, 516 (1988).

[44] J. B. Natowitz, M. Gonin, K. Hagel, R. Wada, S. Schlomo, X. Bin, M. Gui, Y. Lou, D. Utley, T. Botting, R. K. Choudhury, L. Cooke, B. Hurst, D. O'Kelly, R. P. Schmitt, W. Turmel, H. Utsunomiya, G. Nebbia, D. Fabris, J. A. Ruiz, G. Nardelli, M. Poggi, R. Zanon, G. Viesti, R. H. Burch, F. Gramegna, G. Prete, D. Drain, B. Chambon, B. Cheynis, D. Guinet, X. C. Hu, A. Demeyer, C. Pasteur, A. Giorni, A. Lleres, P. Stassi, J. B. Viano, A. Menchaca-Rocha, M. E. Brandan, and P. Gonthier, Nucl. Phys. **A538**, 263c (1992).

[45] M. Gonin, L. Cooke, B. Fornal, P. Gonthier, M. Gui, Y. Lou, J. B. Natowitz, G. Nardelli, G. Nebbia, G. Prete, R. P. Schmitt, B. Srivastava, W. Turmel, D. Utley, H. Utsonomiya, G. Viesti, R. Wada, B. Wilkins, and R. Zanon, Nucl. Phys. **A495**, 139c (1989).

[46] W. E. Ormand, P. F. Bortignon, A. Bracco, and R. A. Broglia, Phys. Rev. C **40**, 1510 (1989).

[47] D. Jouan, B. Borderie, M. F. Rivet, C. Cabot, H. Fuchs, H. Gauvin, C. Grégoire, F. Hanappe, D. Gardès, M. Montoya, B. Remaud, and F. Sébille, Z. Phys. A **340**, 63 (1991).

[48] A. Bonasera, F. Gulminelli, and J. Molitoris, Phys. Rep. **243**, 1 (1994).

[49] A. Bonasera and F. Gulminelli, Phys. Lett. B **259**, 399 (1991).

[50] H. Nifenecker and J. A. Pinston, Annu. Rev. Nucl. Part. Sci. **40**, 113 (1990).

[51] E. Migneco, C. Agodi, R. Alba, G. Bellia, R. Coniglione, A. Del Zoppo, P. Finocchiaro, C. Maiolino, P. Piattelli, G. Russo, P. Sapienza, A. Badalà, R. Barbera, A. Palmeri, G. S. Pappalardo, F. Riggi, A. C. Russo, A. Peghaire, and A. Bonasera, Phys. Lett. B **298**, 46 (1993).

[52] P. Sapienza, R. Coniglione, R. Alba, A. Del Zoppo, E. Migneco, C. Agodi, G. Bellia, P. Finocchiaro, K. Loukachine, C. Maiolino, A. Peghaire, P. Piattelli, and D. Santonocito, Phys. Rev. Lett. **73**, 1769 (1994).

[53] R. J. Vojtech, R. Butsch, V. M. Datar, M. G. Herman, R. L. McGrath, P. Paul, and M. Thoennessen, Phys. Rev. C **40**, R2441 (1989).

[54] B. A. Remington, M. Blann, and G. F. Bertsch, Phys. Rev. Lett. **57**, 2909 (1986).

[55] R. Heuer, B. Müller, H. Stöcker, and W. Greiner Z. Phys. A **330**, 315 (1988).

[56] J. Kasagi and K. Yoshida, in *Proceedings of the 1st Joint Italian-Japanese Meeting on Perspectives in Heavy Ion Physics*, edited by M. Di Toro and E. Migneco (Editrice Compositori, Bologna, 1993), p. 179.

[57] Ph. Chomaz, M. Di Toro, and A. Smerzi, Nucl. Phys. **A563**, 509 (1993).

[58] R. Pittham, Giant Multipole Resonances, Nuclear Science Research Conference Series, 1980 (unpublished), Vol. 1, p. 161.

[59] L. Nilsson, in *Capture Gamma-Ray Spectroscopy and Related Topics*, edited by S. Raman, AIP Conf. Proc. No. 125 (AIP, New York, 1984), p. 125.

[60] F. V. De Blasio, W. Cassing, M. Tohyama, P. F. Bortignon, and R. A. Broglia, Phys. Rev. Lett. **68**, 1663 (1992).

[61] D. R. Chakrabarty, S. Sen, M. Thoennessen, N. Alamanos, P. Paul, R. Schicker, J. Stachel, and J. J. Gaardhøje, Phys. Rev. C **36**, 1886 (1987).

[62] A. Bracco, F. Camera, J. J. Gaardhøje, B. Herskind, and M. Pignanelli, Nucl. Phys. **A519**, 47c (1990).

[63] P. F. Bortignon, M. Braguti, D. M. Brink, R. A. Broglia, C. Brusati, F. Camera, W. Cassing, M. Cavinato, N. Giovanardi, and F. Gulminelli, Nucl. Phys. **A583**, 101c (1995).

[64] M. Thoennessen, Phys. Rev. Lett. **66**, 1640 (1991).

[65] H. P. Morsch, W. Spang, J. R. Beene, F. E. Bertrand, R. L. Auble, J. L. Charvet, M. L. Halbert, D. C. Hensley, I. Y. Lee, R. L. Varner, D. G. Sarantites, and D. W. Stracener, Phys. Rev. Lett. **64**, 1999 (1990).

[66] H. P. Morsch, W. Spang, J. R. Beene, and F. E. Bertrand, Phys. Rev. Lett. **66**, 1641 (1991).

[67] H. Sagawa and G. F. Bertsch, Phys. Lett. **146B**, 138 (1984).

[68] P. F. Bortignon, R. A. Broglia, G. F. Bertsch, and J. Pacheco, Nucl. Phys. **A460**, 149 (1986).